Article

A droplet-based electricity generator with high instantaneous power density

https://doi.org/10.1038/s41586-020-1985-6

Received: 27 May 2019

Accepted: 6 November 2019

Published online: 5 February 2020

Wanghuai Xu[1,2,9], Huanxi Zheng[1,9], Yuan Liu[3,4,9], Xiaofeng Zhou[1,9], Chao Zhang[1], Yuxin Song[1], Xu Deng[5], Michael Leung[6], Zhengbao Yang[1], Ronald X. Xu[2], Zhong Lin Wang[7]*, Xiao Cheng Zeng[3,4]* & Zuankai Wang[1,8]*

Extensive efforts have been made to harvest energy from water in the form of raindrops[1–6], river and ocean waves[7,8], tides[9] and others[10–17]. However, achieving a high density of electrical power generation is challenging. Traditional hydraulic power generation mainly uses electromagnetic generators that are heavy, bulky, and become inefficient with low water supply. An alternative, the water-droplet/solid-based triboelectric nanogenerator, has so far generated peak power densities of less than one watt per square metre, owing to the limitations imposed by interfacial effects—as seen in characterizations of the charge generation and transfer that occur at solid–liquid[1–4] or liquid–liquid[5,18] interfaces. Here we develop a device to harvest energy from impinging water droplets by using an architecture that comprises a polytetrafluoroethylene film on an indium tin oxide substrate plus an aluminium electrode. We show that spreading of an impinged water droplet on the device bridges the originally disconnected components into a closed-loop electrical system, transforming the conventional interfacial effect into a bulk effect, and so enhancing the instantaneous power density by several orders of magnitude over equivalent devices that are limited by interfacial effects.

Our droplet-based electricity generator (DEG) is based on our recent work[19] showing that the continuous impinging of water droplets on a fluorinated material induces a high charge density on its surface. Our DEG device (Fig. 1a) is fabricated using drop-casting of polytetrafluoroethylene (PTFE), deposited with a tiny piece of aluminium, onto a glass substrate coated with indium tin oxide (ITO). As shown in Fig. 1b and Extended Data Fig. 1, the as-fabricated device is optically transparent, smooth and slippery. We hypothesized that, with continuous droplet impinging, the PTFE—a promising electret material with high charge-storage capability and stability[20,21]—could serve as an ideal reservoir for charge storage, while electrostatically inducing opposite charge of the same amount on the ITO for possible charge transfer to an aluminium electrode. We find that when a falling water droplet spreads on the PTFE surface, it bridges the originally disconnected components (the PTFE/ITO and aluminium electrode) into a closed-loop, electrical system.

Figure 1c shows the time-dependent variation of measured surface charges on the PTFE film of an as-fabricated device under a relative humidity of 65.0%. With an increase in the number of impinging tap-water droplets (ion concentration 3.1 mM), there is a gradual increase in the amount of surface charge[19,22]. Eventually, after around 1.6×10^4 droplets, the surface charge reaches a stable value of about 49.8 nC, indicating that continuous droplet impinging can serve as a robust way to maintain stable and sufficient surface charge on the PTFE surface (Extended Data Fig. 2a).

We measured the electricity generation of an individual impinging droplet on the as-fabricated device in which the PTFE surface had been stored with sufficient and stable charges as a result of contact electrification between liquid and solid after continuous droplet impinging up to around 1.6×10^4 times. As shown in Fig. 1d and Supplementary Video 1, 400 commercial light-emitting diodes (LEDs) could be powered to instantaneously light up when four droplets of 100.0 μl each, released from a height of 15.0 cm, contact the device. Focusing on an individual DEG indicates that the open-circuit output voltage and short-circuit current were about 143.5 V (Fig. 1e) and 270.0 μA (Fig. 1f), respectively—around 295.0 and 2,600.0 times higher than the values obtained without an aluminium electrode (Extended Data Figs. 2b, 3). The instantaneous peak power density is 50.1 W m^{-2} under a load resistance of 332.0 kΩ (Extended Data Fig. 2c), which is three orders of magnitude higher than that of the control device without an aluminium electrode. We calculate the average energy-conversion efficiency of our DEG—defined as the harvested electrical energy relative to the input energy of an impinging droplet—to be roughly 2.2%, which is several orders of magnitude higher than that of our control device without an aluminium electrode. Note that the instantaneous peak density can be enhanced further by increasing the surface

[1]Department of Mechanical Engineering, City University of Hong Kong, Hong Kong, China. [2]Department of Precision Machinery and Precision Instrumentation, University of Science and Technology of China, Hefei, Anhui, China. [3]Department of Chemistry, University of Nebraska-Lincoln, Lincoln, NE, USA. [4]Department of Chemical and Biomolecular Engineering, University of Nebraska-Lincoln, Lincoln, NE, USA. [5]Institute of Fundamental and Frontier Sciences, University of Electronic Science and Technology of China, Chengdu, China. [6]School of Energy and Environment, City University of Hong Kong, Hong Kong, China. [7]Beijing Institute of Nanoenergy and Nanosystems, Chinese Academy of Sciences, Beijing, China. [8]Shenzhen Research Institute of City University of Hong Kong, Shenzhen, China. [9]These authors contributed equally: Wanghuai Xu, Huanxi Zheng, Yuan Liu, Xiaofeng Zhou. *e-mail: zhong.wang@mse.gatech.edu; xzeng1@unl.edu; zuanwang@cityu.edu.hk

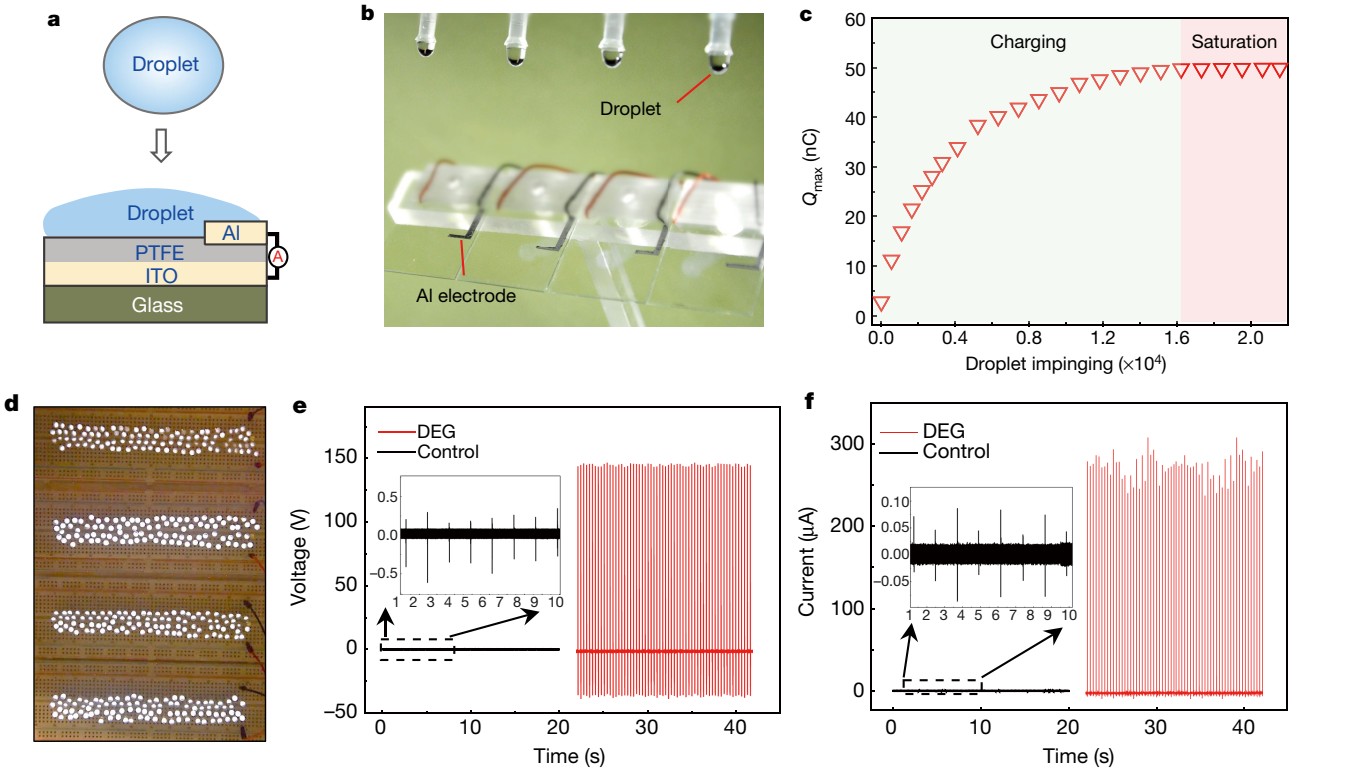

Fig. 1 | Design of the DEG. a, Schematic diagram. **b**, Optical image showing four parallel DEG devices fabricated on a glass substrate. The volume of each droplet is 100.0 μl. **c**, As individual droplets continue to impinge on the as-fabricated device, the amount of charge on the PTFE surface increases gradually and eventually reaches a stable value. **d**, One hundred commercial LEDs can be powered when one droplet, released from a height of 15.0 cm, is in contact with the device. **e**, Under the same experimental conditions (for example, the same droplet size and height of release), the output voltage measured from the DEG (in red, with the frequency of impinging droplets being set at 4.2 Hz, and the total number of droplets being about 84) is more than two orders of magnitude higher than that from the control device (in black, with a droplet frequency of 1.0 Hz, and a total of 20 impinging droplets). The negligible electricity generation from the control device is limited by the interfacial effect, although its PTFE surface is loaded with the same amount of charge as the DEG. **f**, Comparison of output current from the DEG (in red) and the control device (in black) in response to continuous impinging of individual droplets.

charge of the PTFE film using an ion-injection method[23,24] (Extended Data Fig. 4a, b). However, the long-term operation of the DEG device precharged by ion injection is susceptible to a gradual degradation of surface charge, eventually exhibiting performance comparable to that obtained through continuous droplet impact (Extended Data Fig. 4c).

The boost in the output performance of our device compared with the conventional design suggests that the DEG might operate via a different mechanism. First, as shown in Fig. 2a, the essential charges carried by the droplet before and after its impact on the precharged DEG are negligible. Moreover, there is no notable difference in the charge generated by droplets dispensing from a grounded versus an ungrounded outlet[25]. Having ruled out any effects of droplets themselves and of the dropper on electricity generation, we next analysed the time-dependent evolution of the output current (Fig. 2b, c). Initially, upon contact with the PTFE surface, there is no apparent output current from the spreading droplet: the device is in a 'switched-off' state. This is essentially what occurs in the conventional design, with the charge generation being limited by an interfacial effect. The current then exhibits a large acceleration with a pronounced peak of up to 213.7 μA at an on-time (t_{on}) of 0 ms, transitioning into a switched-on state. Careful inspection shows that the sharp increase in the current originates from the contact of the spreading droplet with the aluminium electrode. We propose that this is a result of directional and rapid transfer of charge from the ITO electrode to the aluminium electrode. As plotted in Fig. 2d, in the early stage of droplet spreading, there is a rapid increase in the measured charges—a pattern consistent with the observed current–time curve. As the droplet continues to spread, charge transfer between the ITO and aluminium electrodes continues until the droplet reaches its maximum spreading area, A_{max}, of 2.7 cm^2, which is associated with a maximum charge, Q_{max}, of 49.8 nC (Fig. 2d). With retraction and sliding of the droplet from the impacting centre, the positive current turns to negative, indicating a back flow of charge from the aluminium electrode to the ITO. At an off-time (t_{off}) of 16.0 ms, the water droplet can be fully detached from the slippery aluminium electrode; this is accompanied by the output current and charge dropping to zero (Supplementary Video 2). In this condition, all charge is restored to the ITO, and a new cycle starts. This reversibility is confirmed by the measurement of cyclic charge. As shown in Fig. 2d, the amount of charge transferred between the ITO and aluminium electrodes in each cycle is constant—an indication that there is no deterioration of surface charge on the PTFE film. This is also suggested by the long-term measurement of charge stability (Fig. 1c).

To further understand the mechanisms underlying the performance of our DEG, we next examined the variation in the measured Q_{max} transferred from the ITO to the aluminium electrode as a function of the Weber number (Extended Data Fig. 5). This number is defined as $We = \rho D v^2/\gamma$, where D, v and γ are respectively the diameter, impact velocity and surface tension of the droplet[26–28]. As shown in Fig. 2e, with an increase in the Weber number from 7.7 to 150.4, the transferred charge increases from 13.3 nC to 53.3 nC. Thus, the increase in the amount of transferred charge between the ITO and aluminium electrodes in response to a varying Weber number suggests that the electricity generation is exquisitely regulated by the interaction between the impinging droplet and the configuration of the DEG, rather than

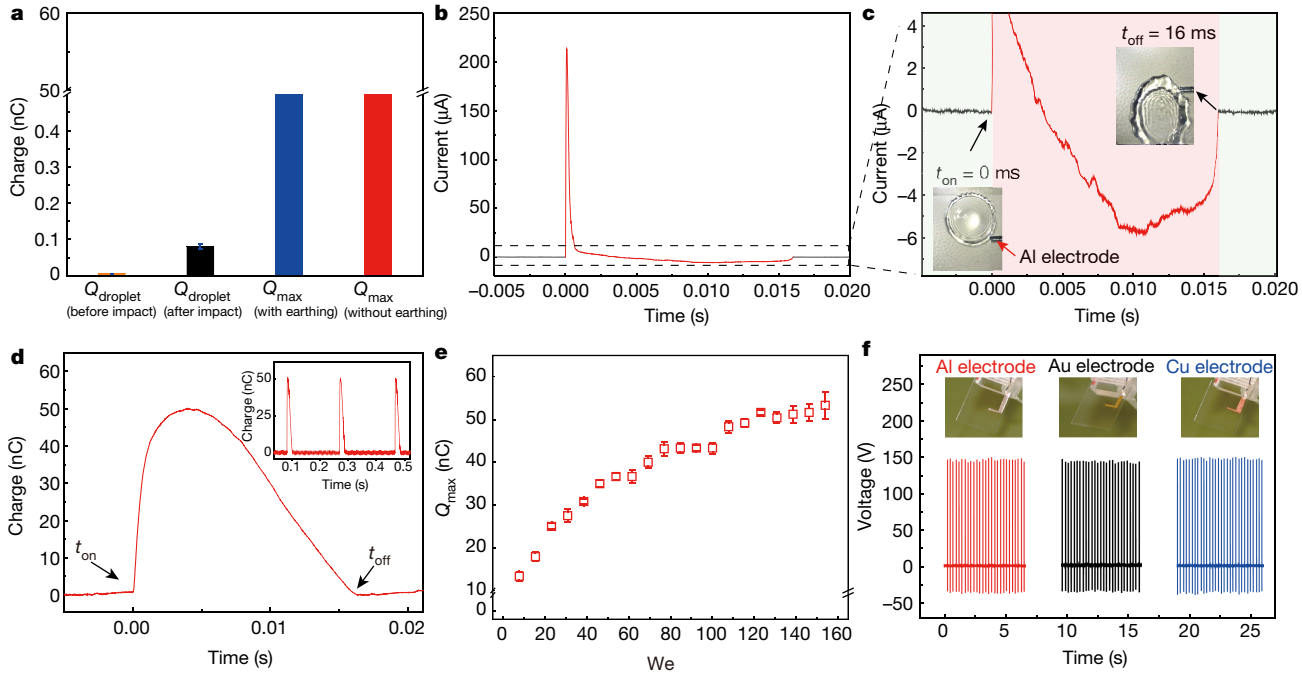

Fig. 2 | Origin of boosted electricity generation. a, The charges carried by the droplet ($Q_{droplet}$) before and after impinging on the PTFE surface are negligible compared with the measured charge of the DEG (Q_{max}). Data are means ± the standard error of the mean (s.e.m.). For each mean, the total number of measurements is around ten. **b**, Time-resolved variation in current generated from the DEG during the entire droplet impact process. The dashed lines delineate the specific part of the current waveform shown in **c**. **c**, Synchronization of droplet-spreading dynamics and current response, and mapping of the time-dependent variation in charge flowing between PTFE/ITO and the aluminium electrode. The droplet retracts but still maintains contact with the aluminium electrode, while the current reverses to a negative value. Insets are snapshots showing droplet dynamics. **d**, Time-dependent variation in the transferred charge, Q, generated on the DEG by an impinging droplet, indicating that the charge can return to zero when the DEG moves to switched-off mode. **e**, Variation in the maximum charge, Q_{max}, generated by an impacting droplet on the DEG under different Weber numbers. Data are means ± s.e.m. For each mean, the total number of measurements is around ten. **f**, Output voltages remain constant when the aluminium electrode is replaced by a gold or silver electrode, suggesting that electricity generation is not sensitive to the specific electrode material. For all specific electrodes, the frequencies of impinging droplets and the total numbers of droplets are 4.2 Hz and about 28, respectively.

originating from just interfacial contact electrification. Moreover, the output is insensitive to the size and spatial location of the aluminium electrode and to the electrode material (Fig. 2f and Extended Data Fig. 6).

Looking at the device from a circuit perspective, the spreading droplet can be treated as a resistor and the PTFE as a capacitor, C_P, in which the water/PTFE serves as the top plate and PTFE/ITO as the bottom plate. In the switched-off mode, no capacitor is formed at the water/

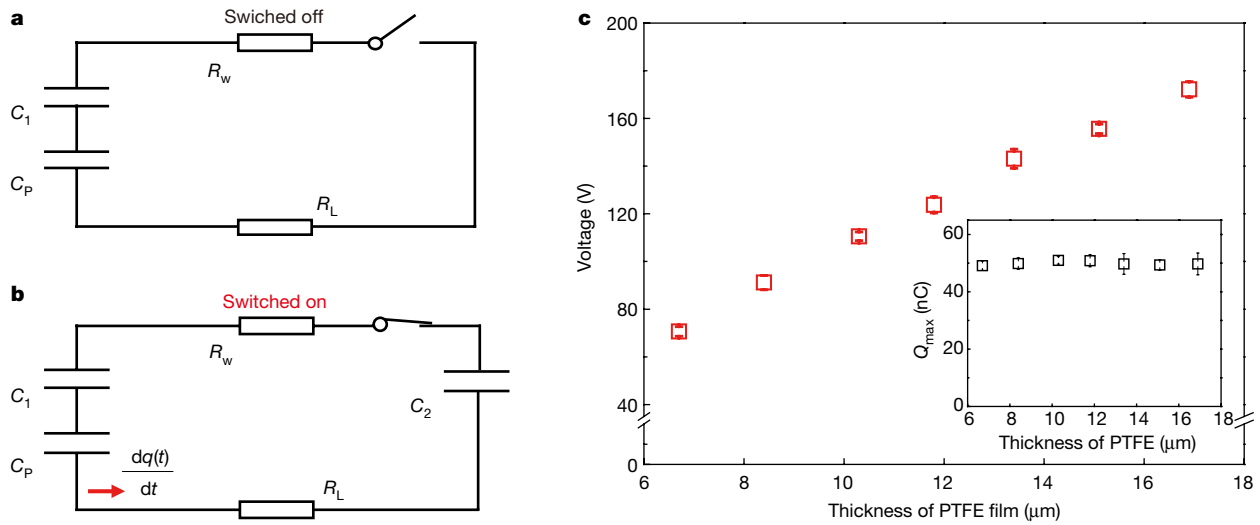

Fig. 3 | Circuit model. a, In the switched-off mode, there is no capacitor formed at the water/aluminium interface. As a result, C_P and C_1 remain in an open circuit and there is no charge flow between them. **b**, When the aluminium electrode and PTFE are connected by the water droplet (switched-on mode), another capacitor, C_2, is established at the water/aluminium interface, forming a closed circuit. R_w, R_L and $dq(t)/dt$ in the circuit are, respectively, the impedance of the water droplet, the impedance of the external load and the derivative of the transferred charge with respect to time. **c**, Output voltage and maximum charge (Q_{max}) as a function of PTFE thickness. Data are means ± s.e.m. For each mean, the total number of measurements is ten.

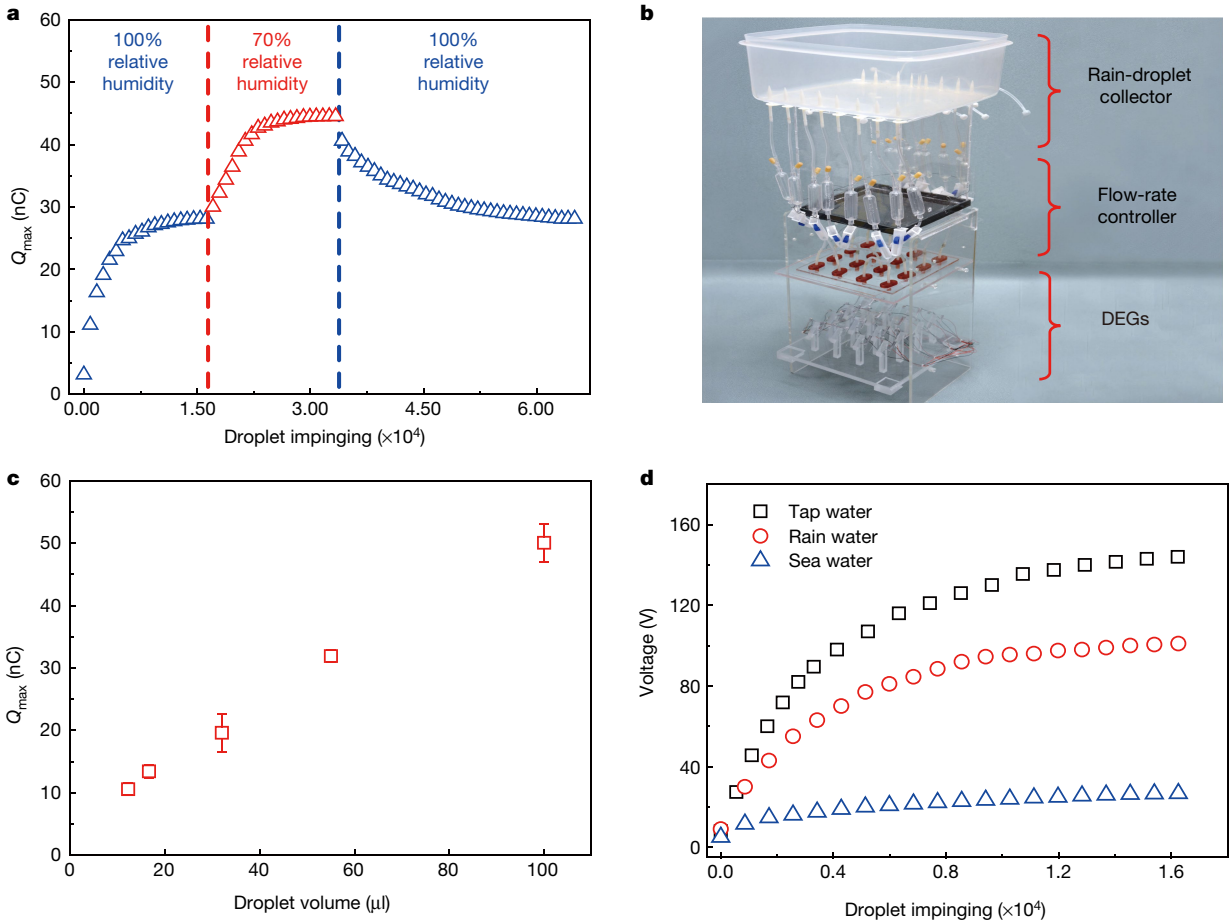

Fig. 4 | Stability and generality. a, Effect of relative humidity on charge loading stability. **b**, Optical image of our system for collecting and dispensing rainwater droplets. **c**, Tailoring the sizes of dispensing droplets for enhanced output. Data are means ± s.e.m. For each mean, the total number of measurements is around ten. **d**, Harvesting of hydrodynamic energy from different water sources: tap water, rainwater and sea water.

aluminium interface, and the circuit maintains an open state (Fig. 3a). By contrast, in the switched-on mode, capacitors are formed at the water/PTFE interface and the water/aluminium interface, transforming the original open circuit into a closed circuit (Fig. 3b). Given that the thickness of the PTFE is several orders of magnitude larger than that of the electric double layer at the water/solid interfaces, the capacitance of the capacitor C_P is negligible compared with that of the capacitors formed at the water/PTFE interface (C_1) and the water/aluminium interface (C_2). In combination with the high-density surface charge stored in the PTFE, the voltage across C_P is dramatically higher than that across C_1 and C_2. Thus, the instantaneous peak output voltage, V, occurs when the spreading droplet is in contact with the aluminium electrode, and can be approximated as $Q_{max}d/(\varepsilon_P A_{max})$, where d and ε_P are respectively the thickness and dielectric constant of the PTFE film. Given a measured A_{max} of 2.7 cm^2 and a Q_{max} of 49.8 nC, we calculate the voltage established across the PTFE to be roughly 143.5 V, consistent with our experimental measurement. Moreover, the measured peak voltage increases linearly with the thickness of the PTFE film, consistent with the predictions of our circuit model (Fig. 3c). Upon completion of the charging process, the C_P capacitor is recharged by the other two capacitors, as observed in current and charge measurements.

To gain molecular-level insights into the process of charge transfer between the PTFE and the aluminium electrode when a water droplet is in contact with both—that is, in the switched-on mode—we carried out molecular-dynamics simulations, using a nanoscale system with a water slab containing positive and negative ions. The simulations predict a concerted motion and rapid separation of mobile positive and negative ions with the presence of an internal electric field between the PTFE and aluminium, once the fixed charges on the PTFE and aluminium are switched on (Extended Data Fig. 7). The separation of the mobile positive and negative charges in the water droplet towards to the water/PTFE interface and the water/aluminium interface, respectively, reveals the charging process of the two capacitors at the water/PTFE interface (C_1) and water/aluminium interface (C_2) at the molecular level.

We also examined the stability of our devices under harsh environments involving high relative humidity[29]. At a relative humidity of 100%, the surface charge increases gradually as the number of impinging droplets increases, reaching a saturated value of 28.1 nC (Fig. 4a). As the relative humidity is reduced to 70%, the surface charge increases rapidly and levels off at a stable value of 44.0 nC. On further exposure to 100% relative humidity, the charge output returns to 28.1 nC, indicating that continuous droplet impinging can help to maintain a constant and steady output even in harsh environments. This enhanced charge stability can be ascribed to the combination of continuous droplet impinging and the good charge-carrying capability of PTFE. By contrast, for control devices made of porous PTFE[21], polydimethylsiloxane (PDMS) or polypropylene, under a relative humidity of 65.0%, performance decays owing to the poor charge stability of the surfaces[30] (Extended Data Fig. 8).

In addition to tap water, our DEG can harvest hydrodynamic energy from both raindrops and sea water. For raindrops, we designed a home-made platform consisting of a droplet collector and a

capillary-tubing-based dispenser (Fig. 4b and Supplementary Video 3). By adjusting the diameter of the capillary tubing and the height of release, we can precisely control the size and velocity of raindrops that contact the DEG arrays for enhanced on-demand output (Fig. 4c). Similarly, such a platform can separate a continuous flow of sea water into discontinuous droplet arrays, allowing for efficient electricity generation from a wide range of water-energy sources. We note that energy conversion from seawater droplets is lower than that from tap water and raindrops; however, it is still much higher than that of the conventional tap-water-based approach (Fig. 4d).

Online content

Any methods, additional references, Nature Research reporting summaries, source data, extended data, supplementary information, acknowledgements, peer review information; details of author contributions and competing interests; and statements of data and code availability are available at https://doi.org/10.1038/s41586-020-1985-6.

1. Lin, Z.-H., Cheng, G., Lee, S., Pradel, K. C. & Wang, Z. L. Harvesting water drop energy by a sequential contact-electrification and electrostatic-induction process. *Adv. Mater.* **26**, 4690–4696 (2014).
2. Jeon, S.-B., Kim, D., Yoon, G.-W., Yoon, J.-B. & Choi, Y.-K. Self-cleaning hybrid energy harvester to generate power from raindrop and sunlight. *Nano Energy* **12**, 636–645 (2015).
3. Xiong, J. et al. Wearable all-fabric-based triboelectric generator for water energy harvesting. *Adv. Energy Mater.* **7**, 1701243 (2017).
4. Jin, S. et al. Large-area direct laser-shock imprinting of a 3D biomimic hierarchical metal surface for triboelectric nanogenerators. *Adv. Mater.* **30**, 1705840 (2018).
5. Xu, W. H. et al. SLIPS-TENG: robust triboelectric nanogenerator with optical and charge transparency using a slippery interface. *Natl Sci. Rev.* **6**, 540–550 (2019).
6. Yu, J., Ma, E. & Ma, T. Exponential energy harvesting through repetitive reconfigurations of a system of capacitors. *Commun. Phys.* **1**, 9 (2018).
7. Wang, Z. L. New wave power. *Nature* **542**, 159–160 (2017).
8. Zhu, G. et al. Harvesting water wave energy by asymmetric screening of electrostatic charges on a nanostructured hydrophobic thin-film Surface. *ACS Nano* **8**, 6031–6037 (2014).
9. Scruggs, J. & Jacob, P. Harvesting ocean wave energy. *Science* **323**, 1176–1178 (2009).
10. Dhiman, P. et al. Harvesting energy from water flow over graphene. *Nano Lett.* **11**, 3123–3127 (2011).
11. Logan, B. E. & Elimelech, M. Membrane-based processes for sustainable power generation using water. *Nature* **488**, 313–319 (2012).
12. Siria, A. et al. Giant osmotic energy conversion measured in a single transmembrane boron nitride nanotube. *Nature* **494**, 455–458 (2013).
13. Feng, J. et al. Single-layer MoS_2 nanopores as nanopower generators. *Nature* **536**, 197–200 (2016).
14. Schroeder, T. B. H. et al. An electric-eel-inspired soft power source from stacked hydrogels. *Nature* **552**, 214–218 (2017).
15. Xue, G. et al. Water-evaporation-induced electricity with nanostructured carbon materials. *Nat. Nanotechnol.* **12**, 317–321 (2017).
16. Huang, Y. et al. Interface-mediated hygroelectric generator with an output voltage approaching 1.5 volts. *Nat. Commun.* **9**, 4166 (2018).
17. Chen, X. et al. Scaling up nanoscale water-driven energy conversion into evaporation-driven engines and generators. *Nat. Commun.* **6**, 7346 (2015).
18. Nie, J. et al. Power generation from the interaction of a liquid droplet and a liquid membrane. *Nat. Commun.* **10**, 2264 (2019).
19. Sun, Q. et al. Surface charge printing for programmed droplet transport. *Nat. Mater.* **18**, 936–941 (2019).
20. Cui, L. et al. The comparative studies of charge storage stabilities among three PP/porous PTFE/PP electret. *J. Electrost.* **67**, 412–416 (2009).
21. Xia, Z., Gerhard-Multhaupt, R., Künstler, W., Wedel, A. & Danz, R. High surface-charge stability of porous polytetrafluoroethylene electret films at room and elevated temperatures. *J. Phys. D* **32**, L83 (1999).
22. Yatsuzuka, K., Mizuno, Y. & Asano, K. Electrification phenomena of pure water droplets dripping and sliding on a polymer surface. *J. Electrost.* **32**, 157–171 (1994).
23. Zhao, P. et al. Emulsion electrospinning of polytetrafluoroethylene (PTFE) nanofibrous membranes for high-performance triboelectric nanogenerators. *ACS Appl. Mater. Interfaces* **10**, 5880–5891 (2018).
24. Wang, S. et al. Maximum surface charge density for triboelectric nanogenerators achieved by ionized-air injection: methodology and theoretical understanding. *Adv. Mater.* **26**, 6720–6728 (2014).
25. Thomson, W. On a self-acting apparatus for multiplying and maintaining electric charges, with applications to illustrate the voltaic theory. *Proc. R. Soc. Lond.* **16**, 67–72 (1868).
26. Liu, Y. et al. Pancake bouncing on superhydrophobic surfaces. *Nat. Phys.* **10**, 515–519 (2014).
27. Bird, J. C., Dhiman, R., Kwon, H.-M. & Varanasi, K. K. Reducing the contact time of a bouncing drop. *Nature* **503**, 385–388 (2013); erratum 505, 436 (2014).
28. Richard, D., Clanet, C. & Quéré, D. Contact time of a bouncing drop. *Nature* **417**, 811 (2002).
29. Nguyen, V. & Yang, R. Effect of humidity and pressure on the triboelectric nanogenerator. *Nano Energy* **2**, 604–608 (2013).
30. Sessler, G. M. in *Electrets* (ed. Sessler, G. M.) 13–80 (Springer, 1980).

Methods

Materials

Acetone (RCI Labscan, 99.5%), ethanol (Sigma Aldrich, 97%), nitric acid (Sigma Aldrich, 70%), porous PTFE film (Sterlitech Corporation, PTU023001), PTFE precursor (Dupont AF 601S2, 6 wt%) and PDMS (Dow Corning Sylgard 184) were used without further purification. The PTFE precursor is composed of PTFE dissolved in 4,5-difluoro-2,2-bis(trifluoromethyl)-1,3-dioxole (a low-boiling organic solvent), which does not contain any extra additives.

Fabrication of DEG device

To fabricate the DEG, we first ultrasonically cleaned a piece of ITO glass slide, of size 30 mm × 30 mm × 0.4 mm, in acetone and then ethanol for 10 min each. We then deposited the PTFE precursor on the ITO glass by drop-casting, and heated it at 120 °C for 15 min to remove all solvent in the PTFE precursor. Upon curing at 120 °C, the PTFE precursor was transformed into a smooth and dense PTFE film, as shown by scanning electron microscopy (SEM; Extended Data Fig. 1). The thickness of the PTFE film can be adjusted by controlling the volume of precursor (Extended Data Fig. 9). To construct the aluminium electrode, we assembled a tiny conductive aluminium tape of size of 1 mm × 5 mm × 50 μm onto the as-prepared PTFE film. For comparison, we also fabricated a control device in the same way but without the aluminium electrode. To fabricate a control device with PDMS film as the dielectric layer, we spin-coated a liquid mix of polydimethylsiloxane and a curing agent (ratio 10/1) with a volume of 200 μl onto ITO glass at a speed of 3,000 revolutions per minute, and then cured the film at 80 °C for 1 h. To fabricate control devices with porous PTFE film and commercial polypropylene tape as the dielectric layer, we attached the porous PTFE film and commercial polypropylene tape directly onto the ITO glass slide.

Characterization and electrical measurement

We used a syringe pump and a plastic tube to generate water droplets. The droplet size could be tailored by varying the inner diameter of the plastic nozzle connecting to the outlet of the plastic tube. The inner diameter of the nozzle required to generate droplets of 100 μl was 6.0 mm. If not specified, the composition of water droplets was tap water at an ion concentration of 3.1 mM. The volume of water droplets was fixed at 100 μl and the droplet outlet was not earthed. We recorded the spreading and retraction dynamics of water droplets using a high-speed camera (Photron FASTCAM SA4) at a typical recording speed of 6,000 frames per second. The voltage output of DEG was measured using an oscilloscope (Rohde and Schwarzrte, RTE1024) equipped with a high-impedance (10 MΩ) probe. We measured the current and the charges transferred between the ITO and aluminium electrode using the oscilloscope coupled with a low-noise current preamplifier (Stanford Research System Model SR570) and a Faraday cup connected with a nanocoulomb meter (Monroe model 284), respectively. The as-fabricated device was tilted at 45.0° for rapid liquid detachment. To measure the variation in maximum charges, Q_{max}, transferred from ITO to aluminium as a function of the Weber number or the maximum spreading area, we varied the releasing heights of droplets between 1 cm and 20 cm. In typical measurements, we kept the relative humidity and the environmental temperature at approximately 65.0% and 20.0 °C, respectively.

Continuous droplet impinging and electricity generation

We showed in the main text that the DEG made of PTFE loaded with sufficient charge allows for reversible and efficient electricity generation. Here we demonstrate that sufficient charge on PTFE can be achieved by continuous droplet impinging. Extended Data Fig. 2a shows the variation in output voltage measured from an individual impinging droplet as a function of the number of droplets impinging. Q_{max} and the output voltage increase gradually with increasing droplet impinging times, eventually reaching a plateau with the charge and voltage stabilized at 49.8 nC and 143.5 V, respectively, after impinging of 1.6×10^4 times (Fig. 1c). This charge-loading method is applicable to a wide range of thicknesses of the PTFE film. Our result shows that the maximum transferred charges are comparable after 1.6×10^4 times of droplet impinging when the thickness of the PTFE film varies from 6.7 μm to 16.9 μm (Fig. 3c). Note that the voltage increases linearly with film thickness, agreeing with the predictions of our circuit model.

Comparison with a conventional generator

We also characterized the performance of a control sample that lacks the aluminium electrode. Note that the PTFE surface of this control was prepared using the same method as for DEG. Extended Data Fig. 3a, b shows an optical image of the as-fabricated droplet-based control device and a schematic drawing of its basic working mechanism[1,4]. Before the droplet contacts the PTFE, the amount of (positive) charges on the ITO is the same as the (negative) charges on the PTFE because of electrostatic induction. Thus, there is no current flow from ITO to the ground (Extended Data Fig. 3b, i). When a water droplet leaves the PTFE surface after impacting (Extended Data Fig. 3b, ii), the droplet becomes positively charged while the PTFE is more negatively charged as a result of contact electrification (Extended Data Fig. 3b, iii)[22]. Accordingly, a flow of current between the ground and ITO electrode is induced (Extended Data Fig. 3b, iv). As shown in Extended Data Fig. 3c, d, the voltage and transferred charge generated from nine droplets impinging on the control device are measured when the frequency of impinging droplets is set at 1.0 Hz. For a single droplet, the output voltage and the amount of transferred charge are roughly −0.4 V and 0.075 nC, respectively, both of which are negligible compared with those of the DEG. Moreover, for the nine droplets, the total amount of transferred charge in the control device is measured to be identical with the accumulated charge carried by the departing droplet (Extended Data Fig. 3d), confirming that electricity generation in the control device indeed originates from the triboelectric effect, a natural interfacial phenomenon. Note that by using continuous droplet impinging or the ion-injection method[23,24], the amount of negative charge on the control PTFE surface can be enhanced, which can then induce positive charges on ITO. However, these positive charges cannot be released from the ITO because of attraction by negative charges on the PTFE, and there is no pronounced electricity generation, in striking contrast to the DEG. All of these results highlight the unique advantage of the DEG, which is characterized by a bulk effect and hence enhanced electricity generation.

Calculation of average conversion efficiency

To quantify the performance of our DEG, we calculated the average conversion efficiency of mechanical energy into electric energy. We first calculated the instantaneous conversion efficiency of the ith droplet impinging, η_i as follows:

$$\eta_i = \frac{E_{out}}{E_{in}} = \frac{\int_{t_{on}}^{t_{off}} \frac{U^2}{R_L} dt}{mgh} \quad (1)$$

where the droplet mass, m, is 0.1 g; the gravitational acceleration, g, is 9.8 m s^{-2}; the relative height between the releasing droplet and the DEG, h, is 15.0 cm; and R_L = 10.0 MΩ. For our DEG, the kinetic energy carried by a droplet (of 100 μl) released from a height of 15.0 cm at the 1.6×10^4th droplet impinging (that is, $i = 1.6 \times 10^4$) is roughly 1.47×10^{-4} J, and the generated electrical energy is calculated as 3.2 μJ (Extended Data Fig. 4b), responding to a η_i of around 2.2%. Such efficiency is five orders of magnitude higher than that of our control device (around 2.1×10^{-5}%).

Next, we discuss the overall conversion efficiency (η_A) of the first n droplets, including those droplets used in precharging; this conversion

efficiency is calculated as the average of the instantaneous conversion efficiency of all droplets ($i = 1, 2, 3, \ldots, n$), expressed as:

$$\eta_A = \frac{\sum_1^n \eta_i}{n} \quad (2)$$

The η_i of individual droplets can be obtained as above (equation (1)). The overall efficiency will increase with the number of impacting droplets. For example, the overall efficiency approaches 2.2%—a conversion efficiency obtained for a single falling droplet impacting on the DEG in the steady state—when the number of impinging droplets is more than 2.0×10^5.

Maximum spreading area

We also studied the dependence of the maximum spreading area, A_{max}, on the surface charge under a fixed impacting Weber number of 100. For a PTFE film without loaded charges, A_{max} is measured at 2.71 cm^2, which is comparable with the A_{max} value measured for PTFE with loaded charges (2.72 cm^2) (Extended Data Fig. 5). This result suggests that the maximum spreading area of a droplet on the PTFE surface relies on the predetermined release height of the impinging droplet, and is insensitive to the surface charge of the PTFE film.

Circuit analysis

We now discuss the entire droplet and device from a circuit perspective[31]. When a droplet spreads on a PTFE surface loaded with sufficient negative charge, the base contact area with the PTFE varies dynamically as a function of time. A capacitor, C_P, is formed with the water/PTFE as the top plate and PTFE/ITO as the bottom plate, respectively. At the water/PTFE interface, there is an additional capacitor, C_1. Before the impinging droplet contacts the aluminium electrode, there is no capacitor formed at the water/aluminium interface. As a result, C_P and C_1 remain in an open circuit and there is no charge flow between them (Fig. 3a). By contrast, when the aluminium electrode and PTFE are connected by the liquid (switched-on mode), the other capacitor, C_2, is established at the water/aluminium interface. Thus, C_1, together with C_P and C_2, form a close circuit. The instantaneous peak output voltage, V, occurs when the spreading droplet is in contact with the aluminium, and can be approximated as $Q_{max}d/(\varepsilon_P A_{max})$. In this circuit, the time-dependent capacitance of C_P, C_1 and C_2 can be expressed as $C_P(t) = A(t)\varepsilon P/d$, $C_1(t) = A(t)\varepsilon_w/\lambda_{EDL}$ and $C_2(t) = A_1(t)\varepsilon_w/\lambda_{EDL}$, respectively, where $A(t)$ and $A_1(t)$ are the time-dependent contact areas of the water/PTFE interface and the water/aluminium interface, respectively; and ε_w and λ_{EDL} are the dielectric constant of PTFE and the width of EDL, respectively. The equivalent circuit is shown in Fig. 3b, governed by the following differential equation:

$$(R_L + R_w)\frac{dq(t)}{dt} = \frac{Q_P(t) - q(t)}{C_P(t)} - \frac{q(t)}{C_1(t)} - \frac{q(t)}{C_2(t)}$$

$$q(t = 0) = 0$$

where $q(t)$ is the transfer charge, and R_L and R_w are the impedance of the external load and water droplet, respectively.

Molecular-dynamics simulations

To simulate ion transport and separation in a water droplet in contact with the as-fabricated device, we carried out molecular-dynamics simulations. To this end, we used the transferable intermolecular potential with four points/for the simulation of water solid ice (TIP4P/ICE)[32] water model, which is popular in molecular-dynamics simulations of water. Various properties of water—including static properties such as the melting point of ice, liquid density in ambient conditions, and water/ice phase diagram, as well kinetic properties such as water's diffusion constant in ambient conditions—have been successfully reproduced using TIP4P/ICE. To mimic ion conduction in tap water, we introduce identical amounts of sodium (Na^+) and chloride (Cl^-) ions into the water. The molecular-dynamics system includes a slab of water containing 4.0×10^4 water molecules with 808 Na^+ and 808 Cl^- ions. To mimic the charged PTFE and aluminium electrode, we use rigid atomic trilayers. We fix 800 negative and 800 positive charges, with a spacing of 8.7 Å, on the middle and bottom atomic layers of PTFE (for the negative charges) and the ITO electrode (for the positive charges) ; each site is charged $+e$ or $-e$. The box size of the model system is 17.3 nm × 17.3 nm × 31.4 nm, in which the thickness of water layer is about 4.5 nm. Periodic boundary conditions are applied in the x and y directions. The parameters for Na^+ and Cl^- are taken from previous work[33] ($\sigma_{Na} = 2.876$ Å; $\varepsilon_{Na} = 0.5216$ kJ mol^{-1}; $\sigma_{Cl} = 3.785$ Å; $\varepsilon_{Cl} = 0.5216$ kJ mol^{-1}; where ε is the depth of a potential well, and σ is the finite distance at which the interparticle potential is zero. The cross Lennard–Jones interaction parameters between water and Na^+ and Cl^- ions are given by the Lorentz–Berthelot rule. The interactions between substrate atoms (sub) and the NaCl water solution are described by the 12-6 Lennard–Jones potential ($\sigma_{Na-sub} = 3.021$ Å; $\varepsilon_{Na-sub} = 0.4785$ kJ mol^{-1}; $\sigma_{Cl-sub} = 3.476$ Å; $\varepsilon_{Cl-sub} = 0.4785$ kJ mol^{-1}; $\sigma_{O-sub} = 3.458$ Å; $\varepsilon_{O-sub} = 0.6223$ kJ mol^{-1}). We used the fast smooth particle-mesh Ewald method to model electrostatic interactions with a real-space cut-off of 10 Å. Van der Waals interactions are truncated at 10 Å. We integrate Newton's equations of motion with a time step of 1 fs by using a leap-frog algorithm in the molecular-dynamics simulations. We use a Nosé–Hoover scheme to maintain the systems at a constant temperature. All molecular-dynamics simulations are carried out using Gromacs 4.5.5 software. First, we perform molecular-dynamics simulations of water with dissolved Na^+ and Cl^- ions but without any charges on the substrates while the temperature is maintained at 300 K. The simulation lasts 3 ns. Next, we perform molecular-dynamics simulations in the constant-temperature and constant-volume ensemble at 300 K for both switched-off and switched-on mode. The simulation lasts 5 ns for each mode.

Data availability

The data that support the findings of this study are available from the corresponding authors on reasonable request.

31. Moon, J. K., Jeong, J., Lee, D. & Pak, H. K. Electrical power generation by mechanically modulating electrical double layers. *Nat. Commun.* **4**, 1487 (2013).
32. Abascal, J., Sanz, E., García Fernández, R. & Vega, C. A potential model for the study of ices and amorphous water: TIP4P/Ice. *J. Chem. Phys.* **122**, 234511 (2005).
33. Koneshan, S. R., Rasaiah, J. C., Lynden-Bell, R. M. & Lee, S. H. Solvent structure, dynamics, and ion mobility in aqueous solutions at 25 °C. *J. Phys. Chem. B* **102**, 4193–4204 (1998).

Acknowledgements Z.W. acknowledges financial support from the National Natural Science Foundation of China (grant 31771083), the Research Grants Council of Hong Kong (grants 11219219, C1018-17G and 11218417), the Shenzhen Science and Technology Innovation Council (grant JCYJ20170413141208098), the Innovation and Technology Council (grants 9440175), and the City University of Hong Kong (grants 9680212 and 9600011). X.C.Z. was supported by the United States National Science Foundation (CHE-1665324). X.Z. was supported by the Science and Technology Committee of the Shanghai Municipality (grant 19511120100) and by Initial Funding for Scientific Research of East China Normal University. Molecular-dynamics simulations were carried out using the computer facility at the University of Nebraska-Lincoln Holland Computing Center.

Author contributions Z.W. and W.X. conceived the research. W.X., H.Z., X.Z. and C.Z. designed the experiments. W.X. prepared the samples. W.X., H.Z. and Y.S. carried out the experiments. Y.L. and X.C.Z. conducted the molecular-dynamics simulations. All authors analysed the data. Z.W., R.X.X., X.D., X.C.Z., W.X., Z.L.W., X.Z., Y.L., M.L., Z.Y. and H.Z. wrote the manuscript.

Competing interests The authors declare no competing interests.

Additional information

Supplementary information is available for this paper at https://doi.org/10.1038/s41586-020-1985-6.

Correspondence and requests for materials should be addressed to Z.L.W., X.C.Z. or Z.W.

Peer review information *Nature* thanks Lars Egil Helseth and the other, anonymous, reviewer(s) for their contribution to the peer review of this work.

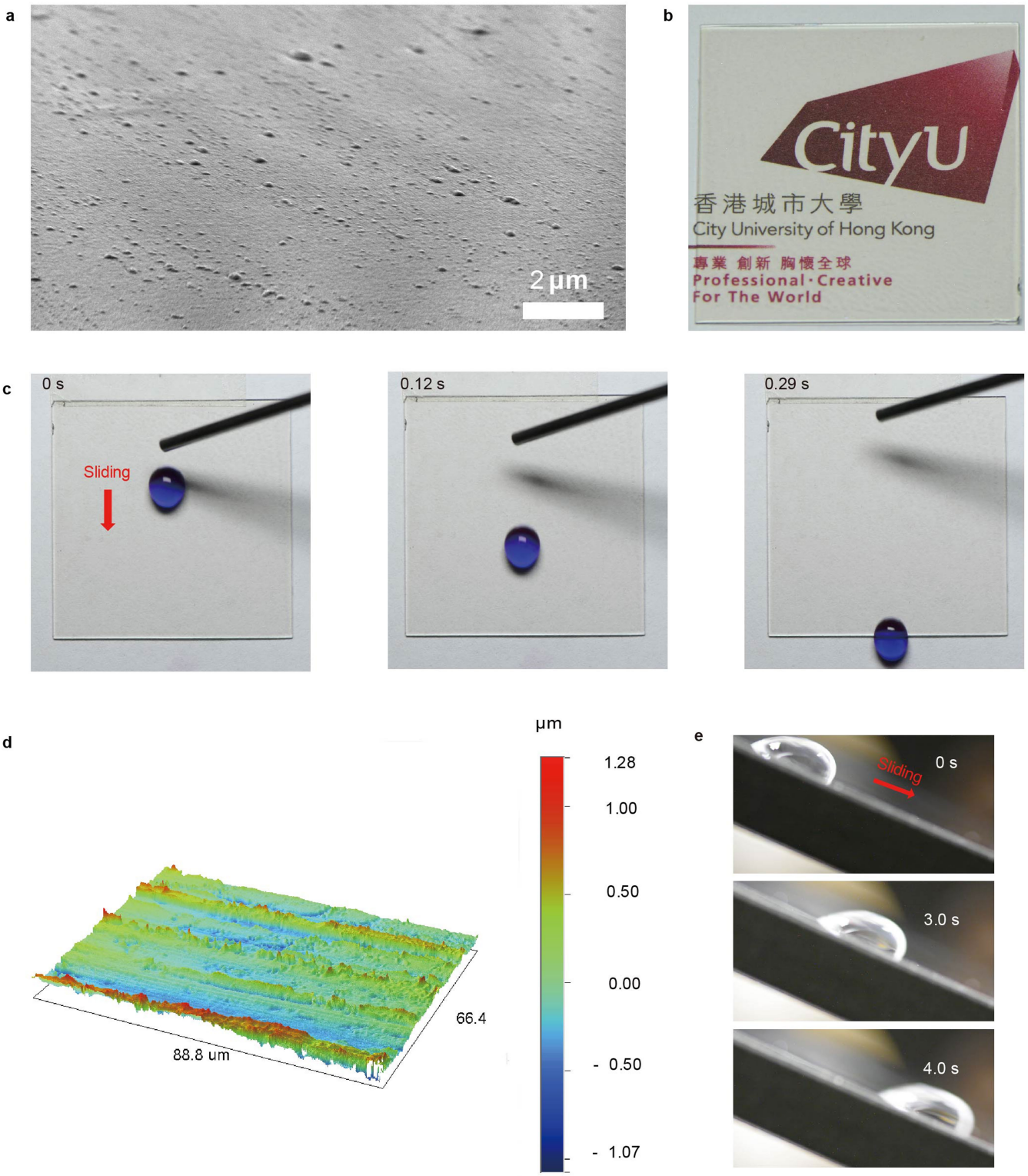

Extended Data Fig. 1 | Surface morphology and sliding behaviour of water droplets on the PTFE film and aluminium electrode. a, SEM image of the PTFE film used in our DEG. Upon curing at 120 °C and solvent evaporation, the PTFE precursor is transformed into a smooth and dense PTFE film. **b**, Photograph of the fabricated PTFE film together with the ITO glass on a logo, showing the high transparency of the film. **c**, A droplet of roughly 30.0 μl can easily slide on the surface of a PTFE film made from pure PTFE solution (placed on a substrate with a tilt angle of 15.0°). **d**, Contour graph image of an aluminium electrode shows that its surface is very flat and uniform. **e**, A droplet can slide off an aluminium electrode without leaving residual water. The aluminium electrode is placed on a substrate with a tilt angle of 25.0°. These is no residual water on the electrode surface.

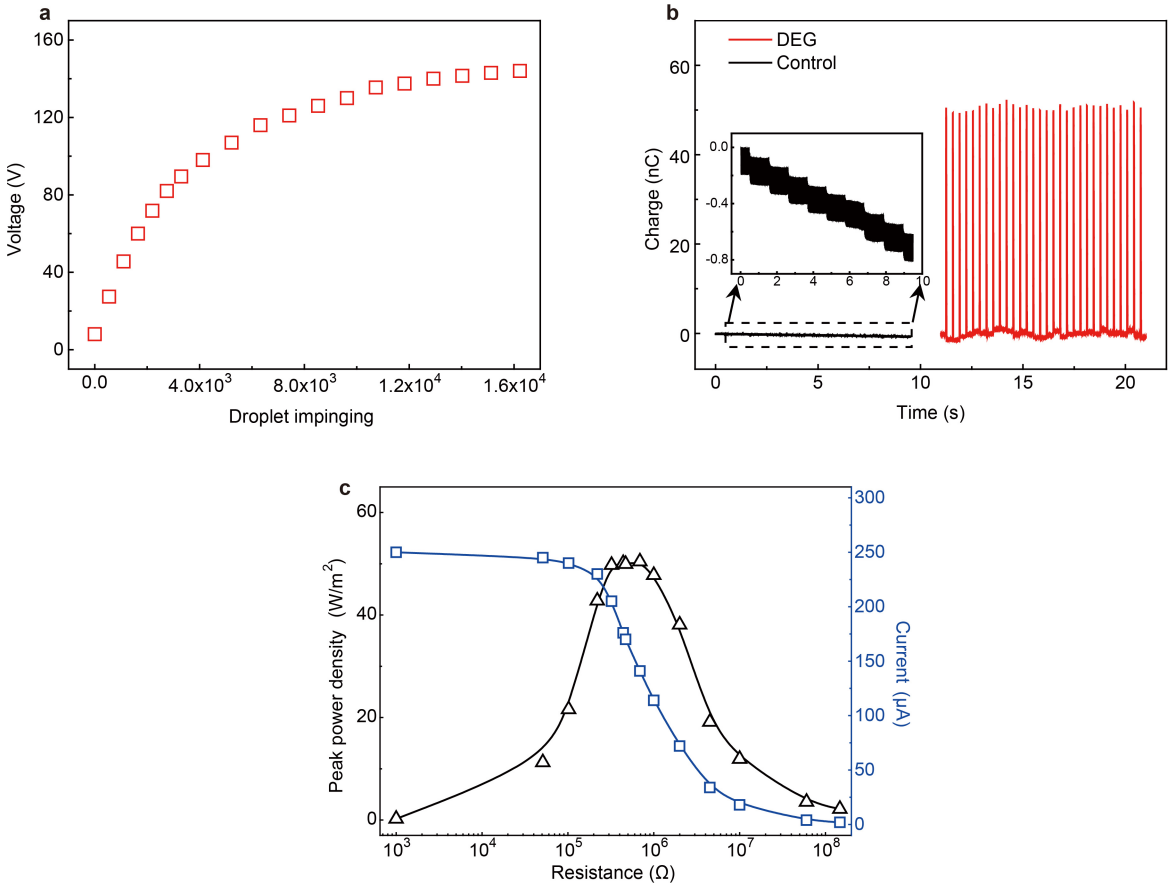

Extended Data Fig. 2 | Surface charging by continuous droplet impinging, and characterization of the output charge and power of the DEG. a, Variation in the output voltage as a function of the number of individual impinging droplets. In this case, the surface was not precharged. The output results purely from charge generation and transfer during droplet impinging. **b**, The output charge measured from the DEG (in red; the frequency of impinging droplets is 4.2 Hz and the total number of droplets is about 42) is roughly 49.8 nC, which is around 640.1 times higher than that of the control device (in black; the frequency of impinging droplets is 1.0 Hz, and the total number of droplets is 9). **c**, When the load resistance increases from 1 kΩ to 100 MΩ, the output current decreases from 250.0 μA to 2.0 μA. When the load resistance is 332.0 kΩ, the peak output power density is 50.1 W m^{-2}.

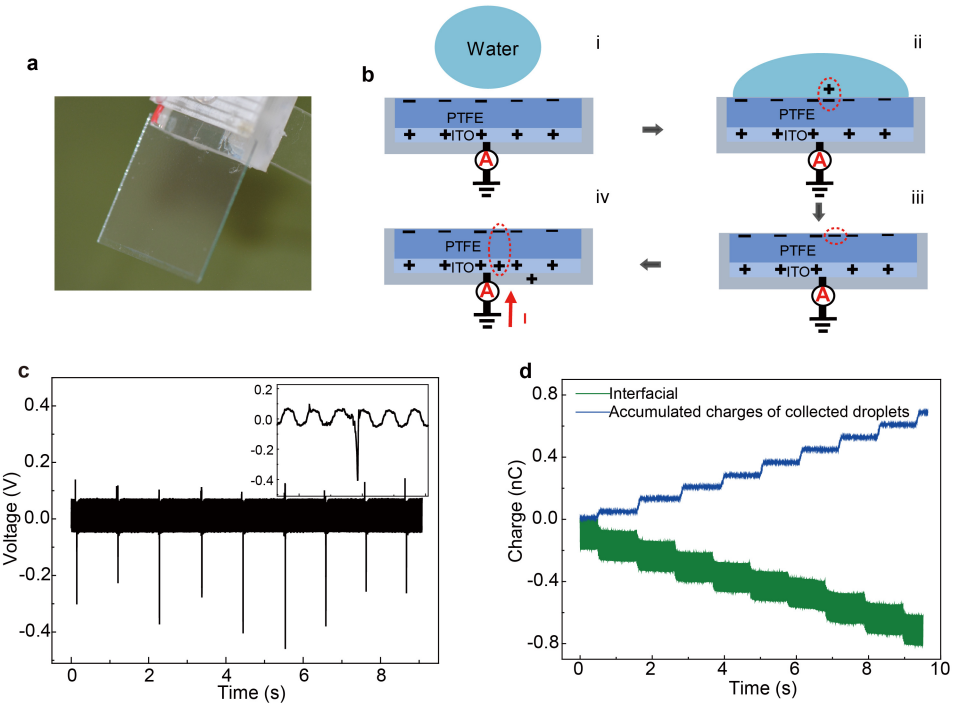

Extended Data Fig. 3 | Control experiment based on a triboelectric nanogenerator. a, Optical image showing the as-fabricated control device. The structure of this control device is similar to that of the DEG, but without an aluminium electrode. **b**, Diagram showing its detailed working mechanism. i, Before the droplet contacts the PTFE, the amount of (positive) charges on the ITO is the same as the (negative) charges on the PTFE, owing to electrostatic induction. Thus, there is no current flow from ITO to the ground. ii, When a water droplet contacts the PTFE surface, the droplet becomes positively charged while the PTFE becomes more negatively charged as a result of contact electrification. iii, When the positively charged droplet leaves, it causes the ITO electrode with positive charges to be unable to screen the more negatively charged PTFE. iv, Accordingly, a flow of current (*I*) between the ground and ITO electrode is induced by electrostatic induction. **c**, Variation in voltage output from the control device as a result of continuous droplet impinging. The inset shows the time-dependent variation in voltage from a single droplet. The frequency of impinging droplets is set at 1.0 Hz, with a total of nine droplets. **d**, In each test of the control device, the amount of transferred charge (in green) is identical to the charge carried by the departing droplets (in blue), showing that electricity generation from the control device indeed originates from contact electrification. The frequency of impinging droplets is 1.0 Hz, with a total of nine droplets.

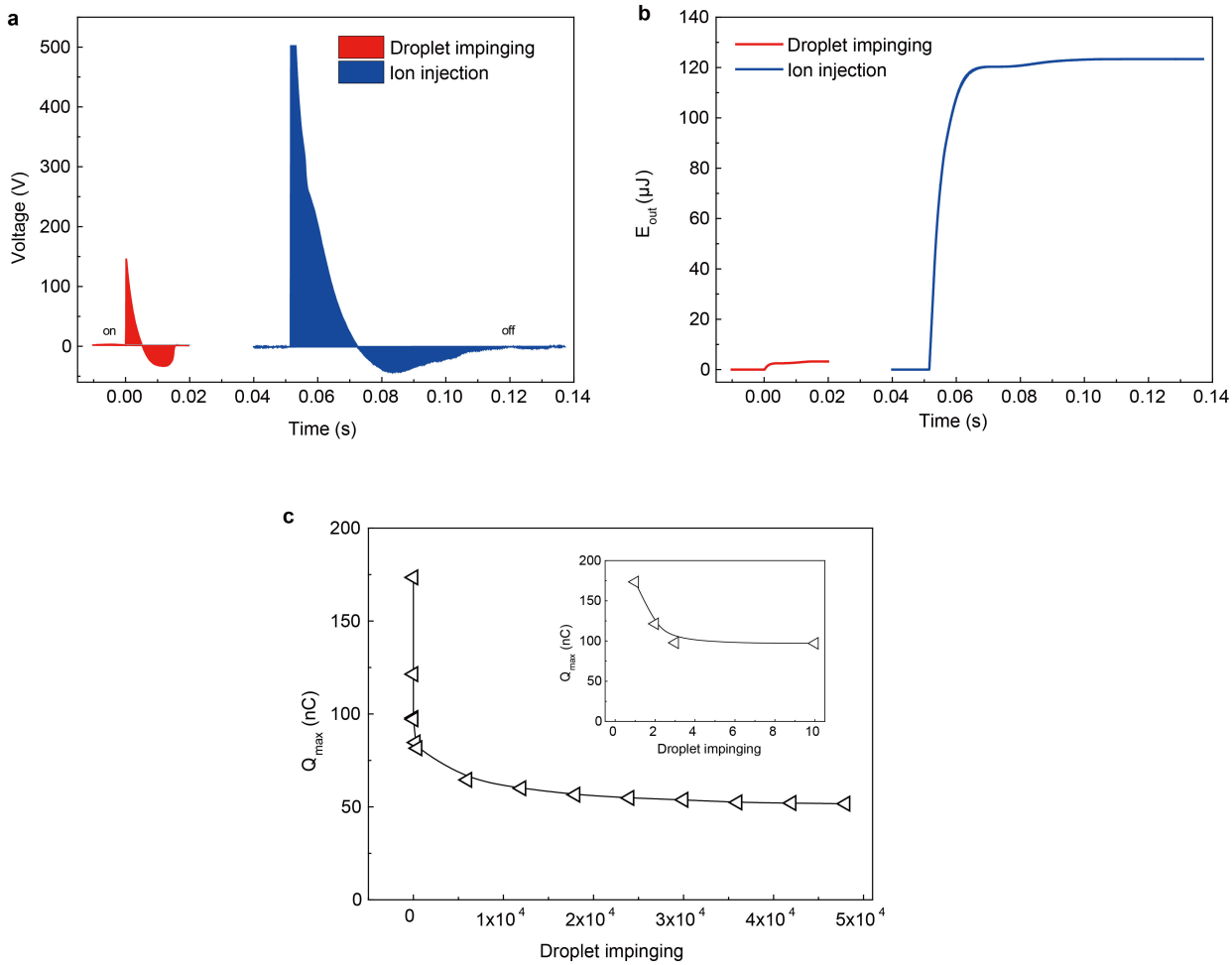

Extended Data Fig. 4 | Enhanced electrical output using the ion-injection method. a, Comparison of the output voltage generated from a single droplet impinging on a DEG that was precharged by droplet impinging (in red) or by ion injection (in blue). **b**, Comparison of the amount of electrical energy (E_{out}) generated from a single droplet impinging on a DEG charged by droplet impinging (in red) or ion injection (in blue). The instantaneous peak density can be enhanced further by increasing the surface charge on the PTFE film through ion injection, using a commercial antistatic gun (Zerostat3, Milty) to inject various ions, including CO^{3-}, NO^{3-}, NO^{2-}, O^{3-} and O^{2-}, from a vertical distance of roughly 5.0 cm. **c**, Variation in the measured maximum charge, Q_{max}, with droplet impinging on a PTFE surface that was precharged using ion injection. Q_{max} decays rapidly and finally reaches a stable value of roughly 49.8 nC. The inset shows the Q_{max} for the first four droplets.

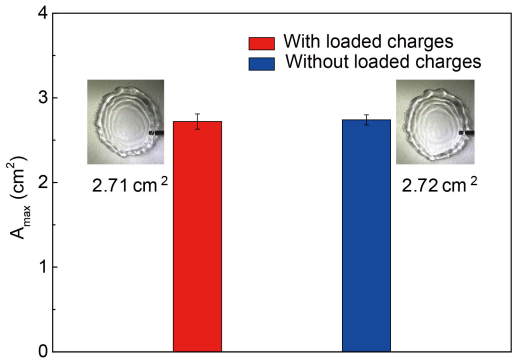

Extended Data Fig. 5 | Effect of surface charge on the maximum spreading area, A_{max}, of a droplet. Data are means ± s.e.m. For each mean, the total number of measurements is ten.

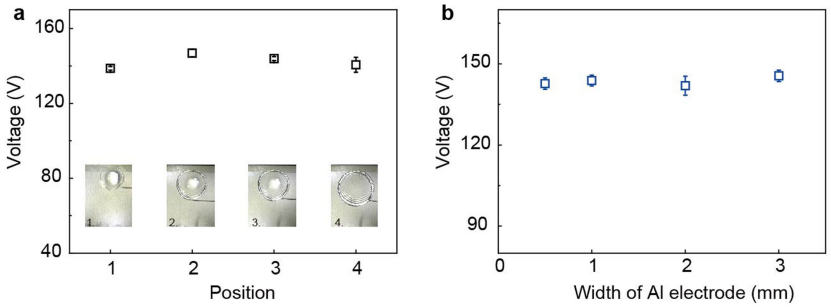

Extended Data Fig. 6 | Effect of the spatial location and width of the aluminium electrode on electricity generation. a, The spatial location of the aluminium electrode was changed, keeping the impact location fixed. In this way, the spacing between the droplet centre and the electrode can be tailored. Insets marked with 1, 2, 3, 4 refer to the four different locations of the aluminium electrode on the PTFE surface. The results show that regardless of the electrode location, the output voltage is constant, suggesting that electricity generation is not sensitive to electrode location. Data are means ± s.e.m. For each mean, the total number of measurements is ten. **b**, The output voltage does not depend on the size of the aluminium electrode. This makes sense because the source of electricity generation is the electrostatically induced charge on the ITO, rather than on the aluminium. Data are means ± s.e.m. For each mean, the total number of measurements is ten.

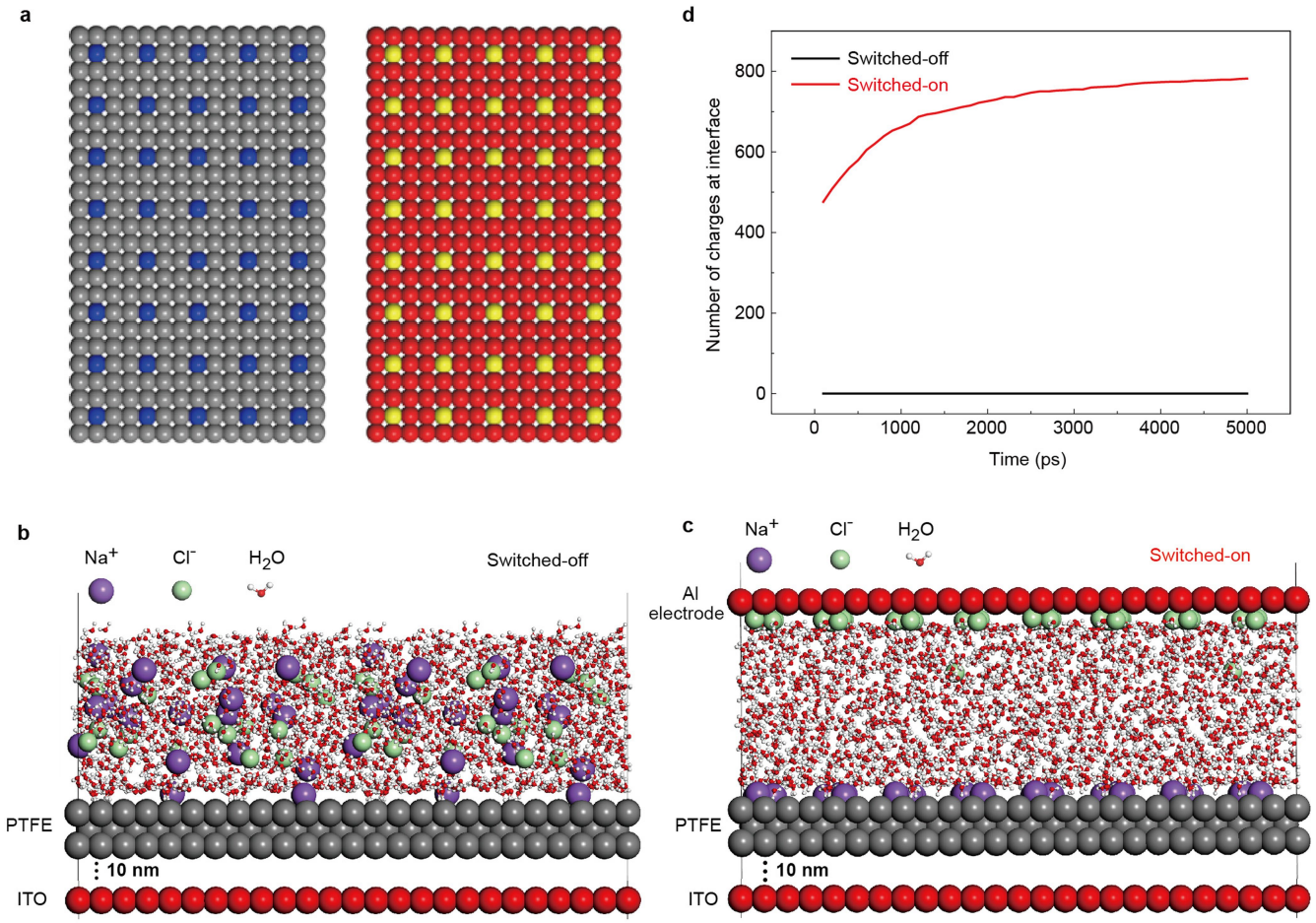

Extended Data Fig. 7 | Molecular-dynamics simulation. a, In the molecular-dynamics simulation, negative (blue) and positive (yellow) charges are fixed on atomic layers of PTFE (grey) and ITO (red), respectively. **b**, Molecular-dynamics simulation showing the distribution of mobile charges (Na^+ and Cl^-) inside the water and on the PTFE surface in switched-off mode (that is, without an aluminium electrode, although the negative and positive charges on PTFE and ITO are turned on). **c**, Molecular-dynamics simulation showing the distribution of charges inside the water and on the PTFE surface in switched-on mode. **d**, Comparison of the number of mobile charges transferred to the water/solid interface in switched-on and switched-off modes.

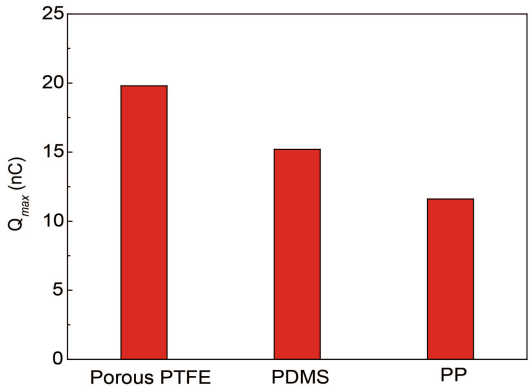

Extended Data Fig. 8 | Control devices made of porous PTFE, PDMS and PP. Comparison of the maximum stable surface charge, Q_{max}, on control devices made of porous PTFE, PDMS and polypropylene (PP) after continuous droplet impact under a relative humidity of 65.0%; all of these charges are much smaller than that of our DEG surface.

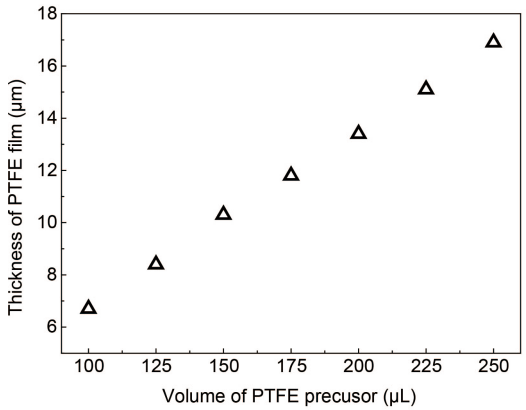

Extended Data Fig. 9 | Thickness of PTFE film as a function of the volume of PTFE precursor. The thickness of the PTFE film increases linearly from 6.7 μm to 16.9 μm as the volume of PTFE precursor increases from 100.0 μl to 250.0 μl.